AlN thin films deposited on different Si-based substrates through RF magnetron sputtering

Xiangquan Jiao · Yu Shi · Hui Zhong ·
Rui Zhang · Jie Yang

Abstract Various Si-based materials such as Si (100), Si (111), oxidized Si (SiO$_2$), and amorphous Si (α-Si) are used as substrates for the growth of c-axis-orientated AlN thin films using radio frequency magnetron sputtering. First, AlN is studied on various substrates under a fixed deposition condition. The results show that AlN deposited on monocrystalline silicon has different structures and stress properties from it deposited on amorphous Si-based layers because of the former's alien growth mechanism at the initiation of growth. Of all the substrates, AlN sputtered on SiO$_2$ exhibits the best structure and morphologies. Then AlN is researched on SiO$_2$ with the RF power and gas flow ratio of N$_2$ to Ar varied. The results approve that among all chosen RF powers, AlN sputtered at 150 W has the strongest (002) crystal peak, the smallest root-mean-square (RMS) surface roughness of 2.74 nm, and the lowest tensile stress of 605 MPa, but the lowest deposition rate. For the gas flow ratio, AlN synthesized at the N$_2$ to Ar flow ratio of 3:1 represents the highest intensity of (002) texture, the smoothest surface with an RMS of 4.21 nm, but the relatively lower deposition rate and larger residual stress.

1 Introduction

Various studies have been conducted on AlN because of its excellent properties, such as wide band gap, desirable chemical and thermal stability, good thermal conductivity, high electrical resistivity, high hardness, and outstanding

X. Jiao (✉) · Y. Shi · H. Zhong · R. Zhang · J. Yang
State Key Laboratory of Electronic Thin Films and Integrated Devices, University of Electronic Science and Technology of China, Chengdu 610054, China
e-mail: xqjiao2008@163.com

acoustic velocity. Thus, AlN is extensively used in applications ranging from optoelectronic devices, insulating layers, electronic packaging, tribological applications, MEMS sensors, and surface/bulk acoustic wave (BAW) resonators [1–3]. The synthesizing methods and deposition conditions of the AlN thin film have been scientifically and extensively studied by many researchers, and the uniform and repeated compounding of a well-textured AlN thin film is not difficult. The main research on AlN thin film focuses on its applications, such as in optical, electrical, acoustic, and mechanical sensors or devices. AlN thin films have been studied on a broad range of substrates, such as Si, metal, sapphire, diamond, GaN, ZnO, PZT, and other insulating ones. Si is the basic material in advanced microelectronics technology and AlN has satisfactory compatibility with IC planar processing [4]; thus, AlN deposited on Si substrate has been mostly studied.

The following four Si-based substrates are common: Si (111), Si (100), SiO$_2$, and α-Si. Many researchers have studied AlN thin films deposited on monocrystalline silicon, such as Si (111) and/or Si (100), using different synthesizing methods [5–8] to investigate the film's crystallizing dynamics and structure. Reports on AlN deposited on SiO$_2$ or α-Si are focused on their functional or structural application in acoustic resonators and MEMS sensors. For examples, SiO$_2$ has been used in BAWs as a temperature compensation layer [9], and SiO$_2$ or α-Si has been used as sacrificial layers for MEMS switches [10, 11]. By contrast, the effects of oxidized silicon or α-Si as seed layers on the crystalline structure and morphologic properties are rarely studied. In fact, some amorphous substrates as seed layers can be used to fabricate high-quality AlN thin films. Artieda et al. [12] obtained a (001)-textured AlN on SiO$_2$ with good texture quality and a piezoelectric $d_{33,f}$ coefficient as high as 5.0 pm/V. Olivares et al. [13] studied AlN on Si$_3$N$_4$, SiO$_2$,

Table 1 AlN sputtering conditions

Parameters	Value
Base pressure (Pa)	$\leq 5 \times 10^{-4}$
Target	Al (99.999 %)
Target substrate distance (cm)	6
N_2/Ar gas flow ratio	1/1, 2/1, 3/1, 4/1
Total gas flow rate (sccm)	60
Sputtering pressure (Pa)	0.65
Sputtering time (h)	2.5
Substrate temperature (°C)	Water cooled
RF power (W)	150, 200, 250, 300

Fig. 1 XRD patterns of AlN thin films deposited on various Si-based substrates by RF magnetron sputtering, the RF power is 200 W and N_2:Ar = 40:20 sccm

amorphous Ta_2O_5, and amorphous TiO_2 and obtained a purely (002)-oriented AlN thin film with low stress and significant piezoelectric activity.

In this paper, the effects of various Si-based substrates on the characteristics of AlN thin films are comprehensively studied. An RF magnetron-sputtering method is used to deposit c-axis-oriented AlN thin films on Si (100), Si (111), SiO_2, and α-Si. RF power and gas flow ratio are varied to study their effects on AlN with SiO_2 as substrates. The crystalline structure, surface microstructure, cross-sectional morphology, and residual stress of AlN thin films are investigated and compared. The growth mechanism of the films is also discussed.

2 Experimental

Two-inch Si (100) and Si (111) wafers were RCA cleaned to remove metallic and organic particles on the surface, followed by dipping for 30 s in 2 % HF to remove the native oxide. Then, the Si (100) wafers were thermally oxidized in wet ambient temperature to obtain a 500 nm-thick silicon dioxide thin film. A 1 μm-thick amorphous silicon film was deposited on a piece of SiO_2 wafer by e-beam evaporation. Thus, four different Si-based substrates were prepared. AlN thin films were synthesized in N_2/Ar reactive atmosphere by RF magnetron sputtering. The deposition conditions are shown in Table 1. Two deposition conditions of RF power and gas flow are varied, while all other parameters are kept constant as shown in the table. Throughout the following results and discussion, only the deposition conditions of RF power and gas flow ratio will be mentioned.

The crystal structure of the AlN thin films was investigated by X-ray diffraction (XRD; Bede, BEDED1 System) with CuKα radiation. The root-mean-square (RMS) surface roughness and surface morphologies of the AlN films were estimated by atomic force microscopy (AFM; Veeco,
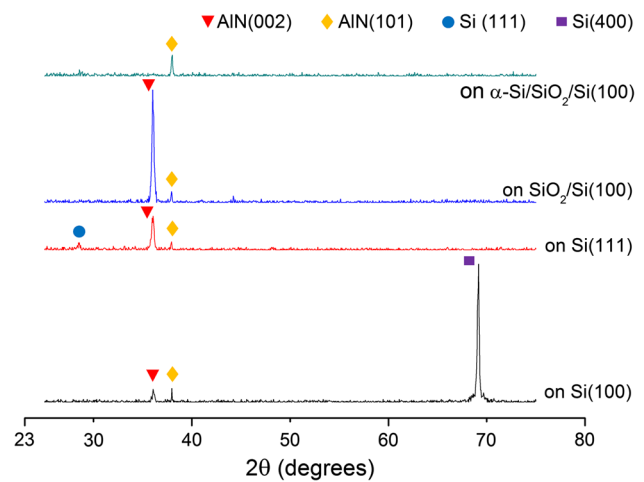
Nanoscope Multimode, Explore). Cross-sectional morphologies were observed by field-emission scanning electron microscopy (FESEM, FEI, INSPECTF). Film residual stresses were tested using the dektak stylus profiler (Veeco, Dektak 150) by measuring the curvature difference between pre- and post-deposited films.

3 Results and discussion

The XRD profiles of AlN thin films sputtered on Si (100), Si (111), SiO_2, and α-Si under 200 W with N_2:Ar = 40:20 sccm are shown in Fig. 1. AlN film deposited on SiO_2 exhibits a sharp and intense c-axis orientation but a slightly weaker orientation on Si (111) and the worst on Si (100). Iriarte et al. [4] also observed that AlN films sputtered on quartz have a narrower film width at half-maximum than on Si substrate. Figure 1 shows that AlN films deposited on crystal Si and SiO_2 exhibit (101) orientation. However, AlN on α-Si does not exhibit the (002) texture but only a single (101) crystallinity. We propose that the high tensile stress of the 1 μm-thick α-Si substrate [14] may induce the (101) plane to easily form at the initiation of growth. The XRD curves of AlN thin films deposited on Si (111) and Si (100) show that AlN on Si (111) has a higher (002) diffraction peak and a nearly negligible (101) peak compared with AlN on Si (100). This result well agrees with that of Zhang et al. [15], who suggests that the preferred orientation of AlN films is more easily controlled on Si (111) than on Si (100) substrates. This preference can be explained by the better matching of AlN (002) plane with a sixfold symmetry Si (111) than a fourfold symmetry Si (100) plane [16]. XRD results further show that SiO_2 substrate is the most suitable for AlN thin film growth. Thus, SiO_2 is chosen
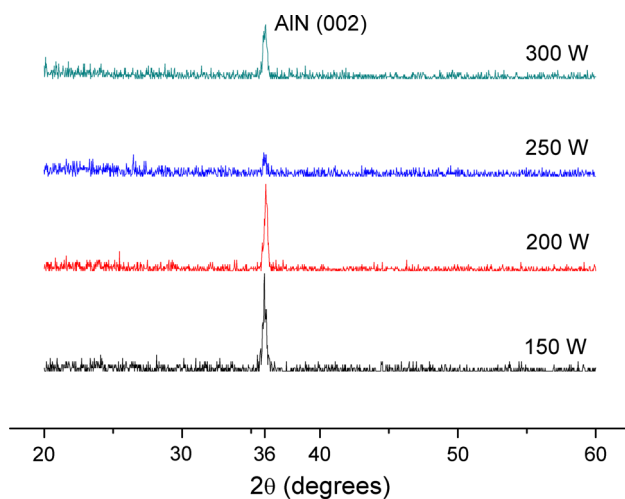
Fig. 2 XRD patterns of AlN thin films sputtered on SiO_2 under different RF power with N_2 flow of 40 sccm and Ar flow of 20 sccm

Fig. 3 XRD patterns of AlN deposited on SiO_2 under 200 W with gas ratio of N_2 to Ar from 1:1 to 4:1. The total flow rate is kept constant to 60 sccm

as substrate to study the effects of RF power and gas flow ratio to the sputtered AlN.

The effects of RF power to the XRD patterns of AlN thin films deposited on SiO_2 are shown in Fig. 2. The gas flow ratio is N_2:Ar = 40:20 sccm. It is evident that all AlN thin films have a single (002) orientation. Under 150 and 200 W the peak intensity of (002) is strong. However, it decreases sharply under 250 W, and then improves a lot at 300 W. This trend of changing on AlN (002) intensity is related to the energy of sputtered AlN adatoms. Under 150 W, the energy of the incident adatoms are too low for them to form the islands. AlN grows in a planar way with new adatom layer stacking on the former one. This growth fashion largely reduces the defects in the film and develops a preferred (002) orientation. With the increase of RF power, incoming adatoms get enough energy to form the small islands, but not high enough to grow into aligned big islands. Increasing the RF power up to 250 W, this phenomenon is obviously manifest and hence a poor c-axis-oriented AlN film is formed. Further increasing the RF power to 300 W, the AlN adatoms have the sufficient energy to diffuse on the substrate surface and form the dense and aligned islands, which results in the improved AlN (002) texture.

Figure 3 shows the XRD patterns of AlN films synthesized under 200 W with different gas ratio of N_2 to Ar. In each deposition the total gas flow rate is 60 sccm. It can be seen from the figure that with N_2:Ar = 1:1, only a minor AlN (110) peak is found. With the increase of N_2 gas flow, a defined AlN (002) crystal peak is observed. Then the peak gets stronger with N_2:Ar = 3:1. Further increasing N_2 flow to 48 sccm (N_2:Ar = 4:1) failed to improve the intensity of AlN (002) peak. These results agree well with the studies of Liu et al. [17]
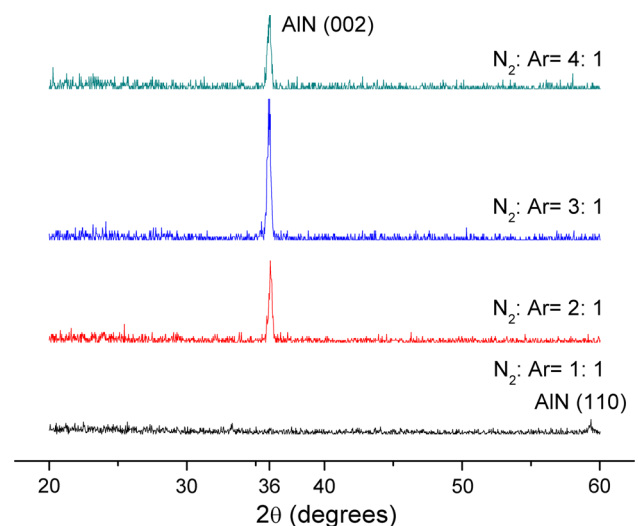
and Kale et al. [18], who both indicate N_2 content plays an important role in the crystal structure of AlN, and a relatively higher proportion of N_2 flow tends to synthesize the (002) direction of AlN. According to our experiments, a moderate gas flow ratio for sputtering the highly oriented AlN (002) is N_2:Ar = 3:1.

To compare the microstructure of AlN thin films, the surface morphologies of various samples were measured by AFM scanning (Fig. 4). The RMS of AlN films on Si (100), Si (111), SiO_2, and α-Si are 6.62, 6.60, 4.22, and 6.69 nm, respectively. AlN thin film on SiO_2 has the lowest surface roughness, whereas the other three films generally have the same roughness between 6.60 and 6.70 nm. The RMS roughness values of Si (100), Si (111), and SiO_2 are below 0.3 nm, which is much smaller than the 1.5 nm roughness of the 1 μm-thick α-Si substrate [14]. Thus, if the surface roughness of α-Si seed layer slightly decreases such as when reducing the film thickness, an AlN film may be obtained on α-Si, which is as smooth as the film on SiO_2. Therefore, AlN thin films deposited on amorphous layers can result in a flatter surface microstructure than on crystal substrates at an equivalent surface level. Similarly, Lee et al. [19] observed that the roughness levels of the as-deposited AlN films are immensely enlarged on crystalline Si and Si_3N_4 in contrast with on SiO_2, though these substrates have small diversities of surface topography. This phenomenon is due to the ability of amorphous layers to reduce lattice mismatch and the shorting range ordering for the growth of these crystallites normal to the substrate at low temperatures [20, 21]. Based on this growth mechanism, crystallites of the AlN thin films deposited on

Fig. 4 Surface morphologies of AlN thin films on different underlying substrates: **a** Si (100), **b** Si (111), **c** SiO₂, and **d** α-Si. The AFM *scanning area* is 2 μm × 2 μm
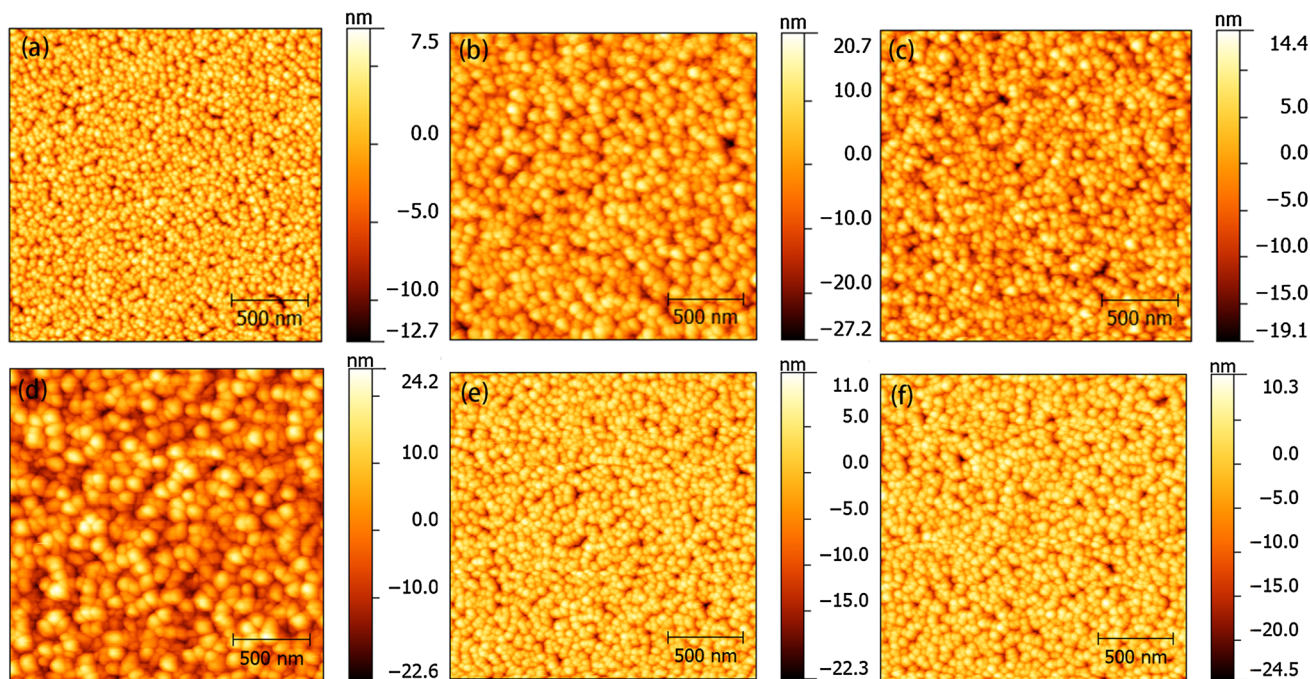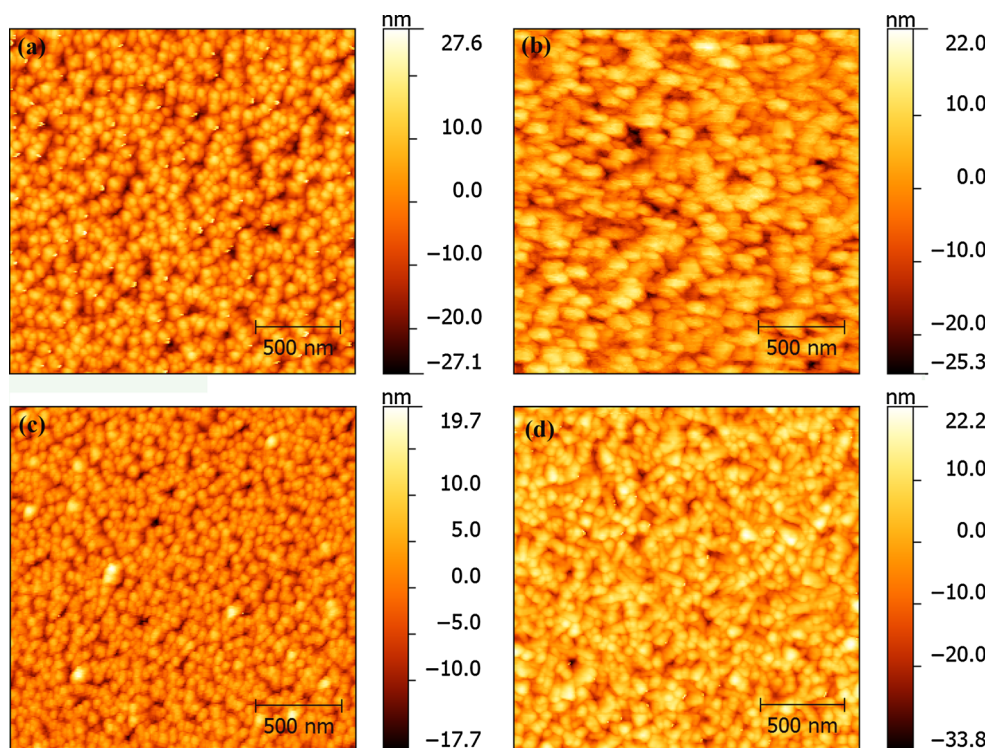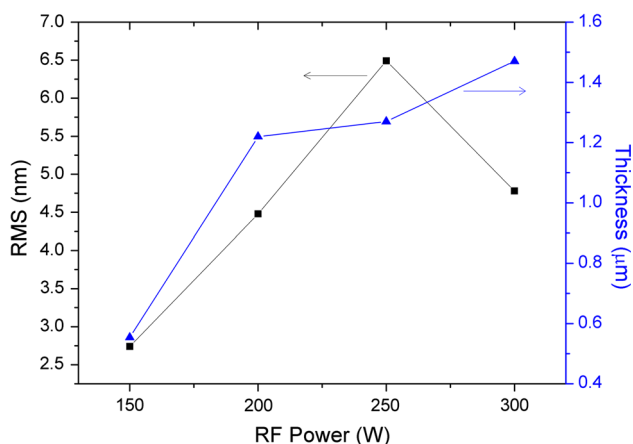

Fig. 5 Surface AFM images of AlN thin films deposited on SiO₂ under different RF power: **a** 150 W, **b** 250 W, and **c** 300 W and at various N₂:Ar ratios: **d** 1:1, **e** 3:1, and **f** 4:1. The AFM *scanning area* is 2 μm × 2 μm

amorphous substrates are aligned to the substrate from the initiation of growth and form a smooth surface at the end of the sputtering process.

To study the influences of RF power and gas flow ratio to the AlN surface microstructure, AFM images are scanned as shown in Fig. 5. Figure 5a–c represent the images of AlN sputtered under 150, 250, and 300 W at gas flow ratio of N₂:Ar = 2:1, respectively. It is evident that AlN prepared at 150 W (Fig. 5a) has the smallest grain size, while at 200 W (Fig. 5b) it has the largest one. The

Fig. 6 RMS and film thicknesses of AlN thin films deposited on SiO₂ as a function of sputtered RF power
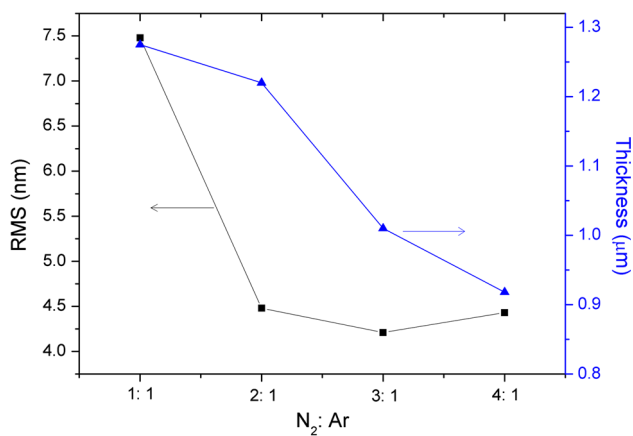
Fig. 7 Surface roughness and film thicknesses of AlN thin films deposited on SiO₂ as a function of N₂ to Ar flow ratio

grain size becomes smaller as the power reaches 300 W (Fig. 5c). The change tendency of AlN surface roughness versus sputtered power is depicted in Fig. 6. The RMS has a close relationship to the grain size and reveals a similar trend: enlarging at first and minishing in the end. At 150 W the AlN film has the smallest RMS of 2.74 nm due to the very small grains. With the increase of RF power the grains grow larger and more defects are formed, which result in the largest RMS of 6.49 nm film at 250 W.

Figure 5d–f are the images of AlN deposited at the N₂ to Ar flow ratios of 1:1, 3:1 and 4:1 under 200 W, respectively. The AlN film has obvious large grain size with the gas ratio of 1:1 (Fig. 5d), while the grain size is greatly shrunk and the films exhibit more homogeneous with the gas ratio increased. The surface morphologies have little differences with the increase of N₂ to Ar ratio from 3:1 (Fig. 5e) to 4:1 (Fig. 5f). The exact data to describe the surface roughness is shown in Fig. 7. It is observed from the plot that the AlN film has an RMS of 7.48 nm at N₂ to Ar flow ratio of 1:1. Then increasing the N₂ to Ar flow ratio to 2:1, the surface roughness is decreased to 4.48 nm. After that the RMS of the films are stabilized at about 4.4 nm. Comparing these results with the XRD patterns in Fig. 3, it can be detected that the AlN (110) film has a rough surface, while the AlN (002) film is much smoother. Once the AlN film has been formed into a single (002) crystal at N₂ to Ar flow ratio of 2:1, more N₂ content will not change the surface roughness enormously.

Many researchers have reported a thin amorphous AlN layer for AlN films deposited on Si by sputtering [20, 22, 23]. Zhang et al. [23] reported that the orientation of the Si (100) and Si (111) substrates has no significant effect on the orientation of deposited AlN films because of the influence of very thin, amorphous-like transition layers between AlN film and two types of crystal Si substrates. The amorphous AlN interlayer between AlN and crystal Si is not beneficial for AlN growth compared with amorphous SiO₂ or α-Si substrates in terms of surface roughness because the AlN interlayer on the Si substrate consists of misoriented AlN crystallites, which causes AlN thin films to deteriorate in the c-axis orientation. However, textured AlN easily grows on the immediate amorphous surface of SiO₂ and α-Si substrates.

SEM images in Fig. 8 represent the effects of substrates on the cross-sectional microstructure of the AlN thin films with a thickness of approximately 1.2 μm. All films show a characteristic columnar morphology normal to the substrate. However, AlN crystalline columns on Si (100) and Si (111) are chunk like and extremely distinct from the needle-shaped columns formed on SiO₂ and α-Si. Substrate surface composition and initial deposition are important for the microstructure in the wurtzite AlN films [23]. In our experiments, the low-temperature deposition induces the nucleation site of AlN to be significantly small. Meanwhile, the low sputtering temperature results in a sufficiently high energy for the AlN molecule to migrate on the substrate, thereby forming dense nucleation sites. These two conditions result in a slender fiber texture of AlN on SiO₂ and α-Si corresponding to zone T of Thornton's diagram [24].

Regarding AlN grown on Si (100) and Si (111), a misoriented interlayer is formed between AlN and crystal Si substrate because of lattice mismatch at a low temperature. This interlayer leads to cross-growth of AlN (002) crystallites from the initiation of growth. Thus, large AlN columns are created because of this intertexture of AlN crystallites. The subsequent growth of (002)-axis AlN films is consistent with this trend, and a chunk-like columnar structure is formed.

The cross-sectional view of AlN films is shown through SEM images in Fig. 9. All films exhibit a columnar
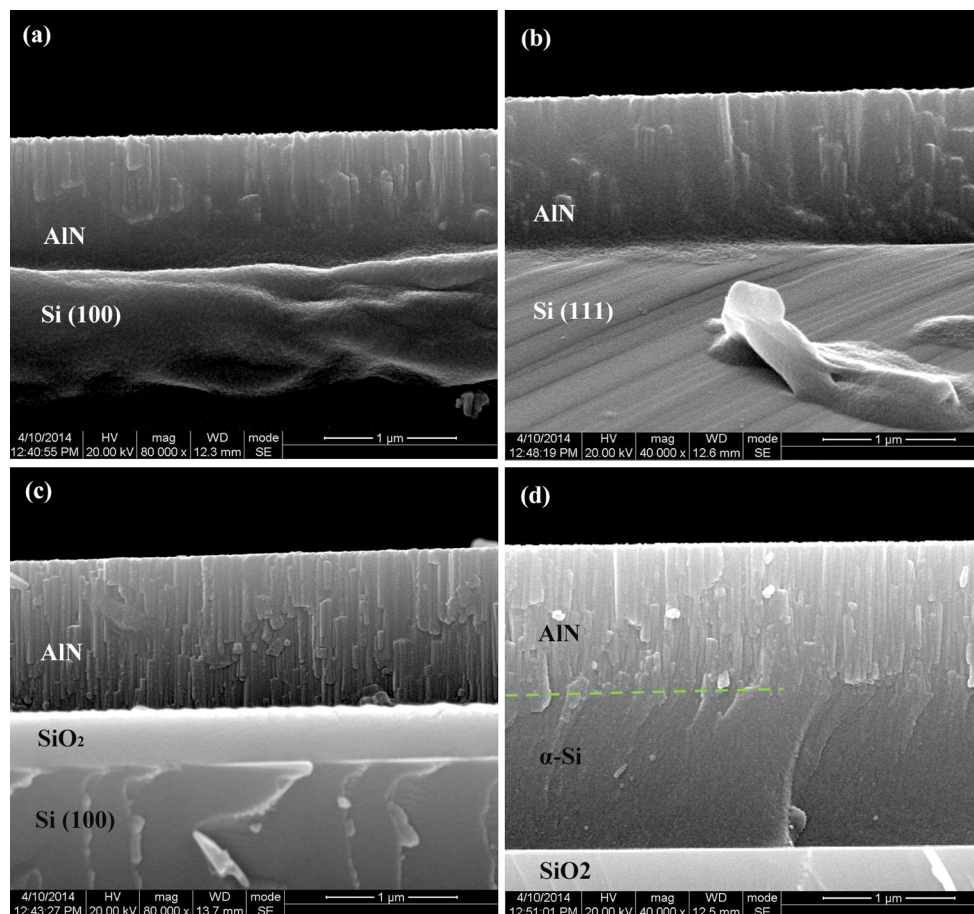
Fig. 8 Cross-sectional SEM images of 1.2 μm-thick AlN thin films deposited on various substrates: **a** Si (100), **b** Si (111), **c** SiO$_2$/Si (100), and **d** α-Si/SiO$_2$/Si (100)

structure, however, the film thickness, column width, and column arrangement are not the same. Cross-sectional micrographs of AlN films affected by RF power of 150, 250, and 300 W correspond to Fig. 9a–c, respectively. It is observed that the film thickness increases a lot from 0.554 μm at 150 W to 1.47 μm at 300 W. This is because the higher power will improve the energy of the incoming ionized species and reduce the rearrangement time of the adatoms on the substrate surface before arrival of next atoms [18]. It also can be seen from Fig. 9 that AlN film sputtered at 250 W (Fig. 9b) has the crushed columns compared to the films deposited at 150 W (Fig. 9a) and 300 W (Fig. 9c), which is indicative of a poor oriented crystal structure for the AlN film, similar to the XRD patterns as shown in Fig. 2. In contrast to the RF power, the N$_2$ content has a negative influence to the film thickness. At a N$_2$ to Ar flow ratio of 1:1, the AlN film is 1.275 μm (Fig. 9d). Increasing the N$_2$ flow ratio will generate more ionized particles and enhance the collision probability, and hence reduce the energy and number of incoming ions to the surface. As a result, the AlN thickness decreases to 1.03 μm when the N$_2$ to Ar flow ratio reaches 3:1 (Fig. 9e).

Following this changing trend, the film is declined to 0.918 μm at N$_2$ to Ar flow ratio of 4:1 (Fig. 9f). To examine the microstructure, it is observed from Fig. 9d that the AlN film has the indistinct columnar structure and a lot of pebble like grains embedded among the columns, which suggests a poor crystal texture, corresponding to the XRD pattern shown in Fig. 3. The columns are refined and clearly seen with the increase of N$_2$ content as shown in Fig. 9e, indicating a well-orientated crystallinity. Further increasing the N$_2$ to Ar flow ratio to 4:1, some narrow gap is visible between the adjacent columns, and in some regions the columns are combined into large chunk, demonstrating a declined AlN (002) crystal orientation. From the above talk, it can be concluded that the crystal structure of the sputtered AlN thin films reflected through the SEM images agrees well with the XRD patterns as shown in Fig. 3. The thickness changing curves of AlN films with RF power and N$_2$ to Ar flow ratio as different variables are depicted in Figs. 6 and 7, respectively.

Residual stress is an important characteristic of thin films because it alters the energy-band structure and can influence the film properties, even resulting in film
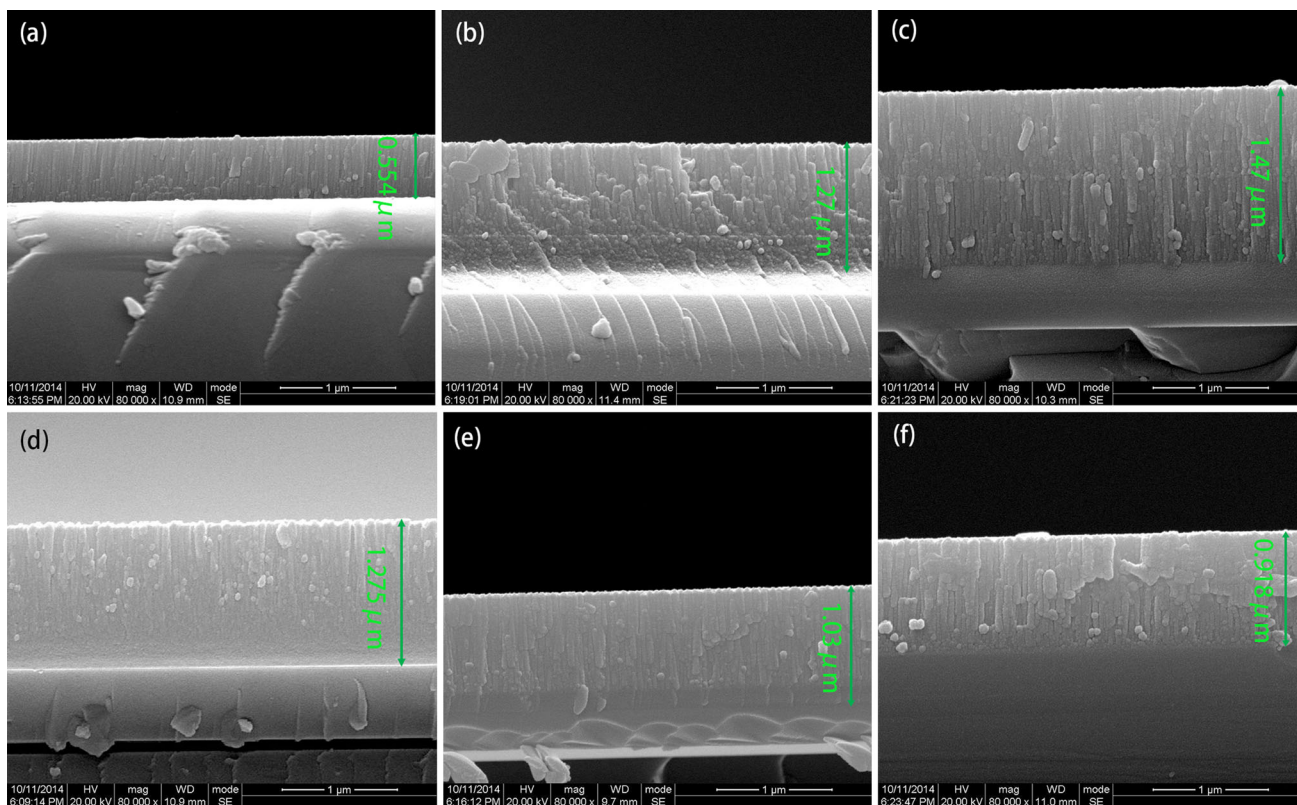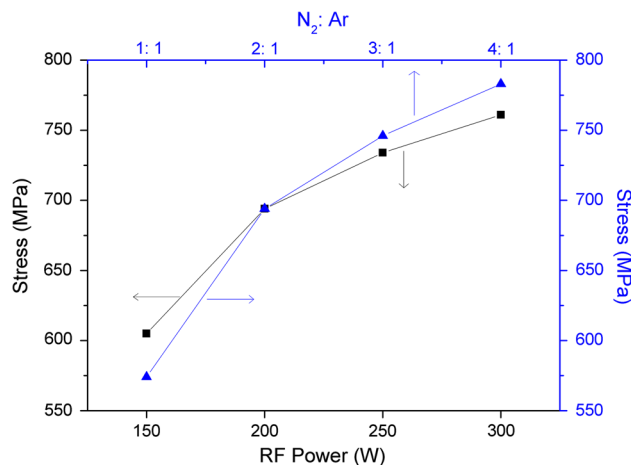
Fig. 9 Cross-sectional SEM images of AlN films on SiO$_2$ under various RF power: **a** 150 W, **b** 250 W, and **c** 300 W and at various N$_2$:Ar flow ratios: **d** 1:1, **e** 3:1, and **f** 4:1
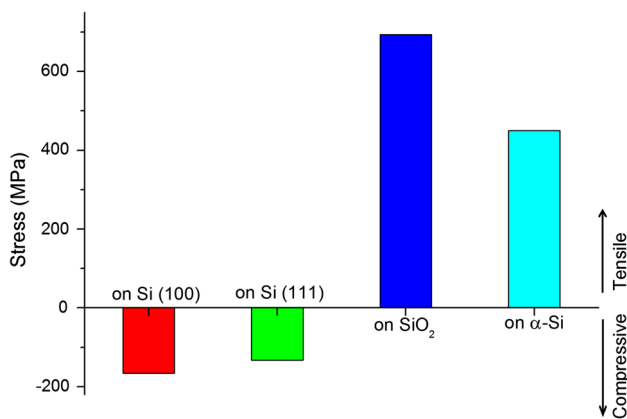
Fig. 10 Residual stresses of AlN thin films deposited on different substrates

Fig. 11 Two different residual stress *curves* of AlN thin films: one is as a function of RF power and the other is as a function of N$_2$ to Ar flow ratio

cracking [25]. The residual stresses of AlN thin films deposited on crystal Si and amorphous substrates are diagramed in Fig. 10. The residual stresses of the AlN films on Si (100) and Si (111) are −166 and −133 MPa, respectively, exhibiting compressive stress, whereas these residual stresses are 694 and 450 MPa on SiO$_2$ and α-Si, exhibiting a tensile type. These stress characteristics of AlN thin films are related to their microstructures. As shown in Fig. 8, the columnar AlN crystallites on Si (100)

and Si (111) are very wide such that a small amount of grain boundaries are induced; thus, a dense film structure is formed. For AlN grown on SiO$_2$ and α-Si, the slender fiber texture results in plenty of grain boundaries, which forms a relatively non-compact columnar structure associated with

tensile stress. Therefore, the residual stress of AlN thin film is closely related to crystalline structure.

The stresses of AlN thin films separately affected by RF power and by N_2 to Ar flow ratio are plotted in Fig. 11. All films exhibit a tensile type stress. For the RF power, the residual stress is dominated by the film thickness; for the N_2 to Ar flow ratio, it is most influenced by the energy of the incident atoms. Thus, the residual stresses both exhibit an elevating trend with the increase of RF power and the N_2 to Ar flow ratio.

4 Conclusions

This paper explores two directions to study the AlN thin films under a water-cooled condition through RF magnetron sputtering. First is that the effects of various Si-based substrates on the characteristics of as-deposited AlN thin films. XRD patterns show that AlN thin films grown on three other substrates exhibit a c-axis orientation associated with a weak (101) texture, except for AlN deposited on α-Si with a (101) texture. The smallest surface roughness of 1.2 μm-thick AlN film is obtained on SiO_2 with an RMS roughness of 4.22 nm. Cross-sectional morphologies and residual stresses demonstrate a different growth mechanism for AlN deposited on monocrystalline Si and amorphous Si-based layers. AlN films deposited on monocrystalline Si exhibit low compressive residual stress, whereas films on amorphous layers have a large tensile residual stress. Thus, we consider SiO_2 as the most appropriate candidate for the growth of well-textured AlN thin films with low surface roughness.

The second direction is using SiO_2 as the substrate to study the effects of RF power and N_2 to Ar flow ratio on the sputtered AlN thin films. After a series of discussion on the structure, morphologies, and residual stress, it is found that AlN thin film sputtered under 150 W has the best (002) texture, the smoothest surface, and smallest tensile stress, but the lowest deposition rate. For AlN thin films sputtered at various N_2 to Ar flow ratios, it is observed that the strongest (002) crystal peak is obtained at a ratio of 3:1, which is also the gas flow condition to achieve the smallest RMS. However, the deposition rate under this condition is a little lower and the residual stress is slightly higher.

References

1. U. Figueroa, O. Salas, J. Oseguera, Surf. Coat. Technol. **200**, 1768 (2005)
2. Z.X. Bi, Y.D. Zheng, R. Zhang, S.L. Gu, X.Q. Xiu, L.L. Zhou, B. Shen, D.J. Chen, Y. Shi, J. Mater. Sci. Mater. Electron. **15**, 317 (2004)
3. S. Marauska, V. Hrkac, T. Dankwort, R. Jahns, H.J. Quenzer, R. Knöchel, L. Kienle, B. Wagner, Microsyst. Technol. **18**, 787 (2012)
4. G.F. Iriarte, J.G. Rodríguez, F. Calle, Mater. Res. Bull. **45**, 1039 (2010)
5. R.D. Vispute, J. Narayan, H. Wu, K. Jagannadham, J. Appl. Phys. **77**, 4724 (1995)
6. G.F. Iriarte, D.F. Reyes, D. González, J.G. Rodriguez, R. García, F. Calle, Appl. Surf. Sci. **257**, 9306 (2011)
7. E. Milyutin, S. Harada, D. Martin, J.F. Carlin, N. Grandjean, V. Savu, O. Vaszquez-Mena, J. Brugger, P. Muralt, J. Vac. Sci. Technol. B **28**, L61 (2010)
8. A. Szekeres, Z. Fogarassy, P. Petrik, E. Vlaikova, A. Cziraki, G. Socol, C. Ristoscu, S. Grigorescu, I.N. Mihailescu, Appl. Surf. Sci. **257**, 5370 (2011)
9. J. Bjurström, G. Wingqvist, V. Yantchev, I Katardjiev. J. Micromech. Microeng. **17**, 651 (2007)
10. J. Olivares, E. Iborra, M. Clement, L. Vergara, J. Sangrador, A. Sanz-Hervás, Sens. Actuators A **123–124**, 590 (2005)
11. C.K. Chung, M.Q. Tsai, P.H. Tsai, C. Lee, J. Micromech. Microeng. **15**, 136 (2005)
12. A. Artieda, C. Sandu, P. Muralt, J. Vac. Sci. Technol. A **28**, 390 (2010)
13. J. Olivares, J. Capilla, M. Clement, J. Sangrador, E. Iborra, IEEE international ultrasonics symposium proceedings, (IEEE, Orlando, FL, 2011), p. 1716
14. X.Q. Jiao, R. Zhang, J. Yang, H. Zhong, Y. Shi, X.Y. Chen, J. Shi, Appl. Phys. A **116**, 621 (2014)
15. J.X. Zhang, H. Cheng, Y.Z. Chen, A. Uddin, S. Yuan, S.J. Geng, S. Zhang, Surf. Coat. Technol. **198**, 68 (2005)
16. K. Dovidenko, S. Oktyabrsky, J. Narayan, M. Razeghi, J. Appl. Phys. **79**, 2439 (1996)
17. W.K. Liu, K.W. Tay, S.C. Kuo, M.J. Wu, Sci. China Ser. G **52**, 226 (2009)
18. A. Kale, R.S. Brusa, A. Miotello, Appl. Surf. Sci. **258**, 3450 (2012)
19. S.H. Lee, J.K. Lee, K.H. Yoon, J. Vac. Sci. Technol. A **21**, 1 (2003)
20. G.W. Auner, F. Jin, V.M. Naik, R. Naik, J. Appl. Phys. **85**, 7879 (1999)
21. Y.J. Yong, J.Y. Lee, H.S. Kim, J.Y. Lee, Appl. Phys. Lett. **71**, 1489 (1997)
22. U. Kaiser, P.D. Brown, I. Khodos, C.J. Humphreys, H.P.D. Schenk, W. Richter, J. Mater. Res. **14**, 2036 (1999)
23. J.X. Zhang, Y.Z. Chen, H. Cheng, A. Uddin, S. Yuan, K. Pita, T.G. Andersson, Thin Solid Films **471**, 336 (2005)
24. J.A. Thornton, Ann. Rev. Mater. Sci. **7**, 239 (1977)
25. R.E. Sah, L. Kirste, M. Baeumler, P. Hiesinger, V. Cimalla, V. Lebedev, H. Baumann, H.-E. Zschau, J. Vac. Sci. Technol. A **28**, 394 (2010)